International Journal of Nanomedicine

Dovepress
open access to scientific and medical research

Open Access Full Text Article

ORIGINAL RESEARCH

Ta-Coated Titanium Surface With Superior Bacteriostasis And Osseointegration

This article was published in the following Dove Press journal:
International Journal of Nanomedicine

Xiao-Meng Zhang*
Yuan Li*
Ying-Xin Gu
Chu-Nan Zhang
Hong-Chang Lai
Jun-Yu Shi

Department of Implant Dentistry, National Clinical Research Center for Oral Diseases, Shanghai Key Laboratory of Stomatology, Shanghai Ninth People's Hospital, Shanghai Jiao Tong University School of Medicine, Shanghai 200011, People's Republic of China

*These authors contributed equally to this work

Background: Although tantalum (Ta)-based coatings have been proven to have good antibacterial activity, the underlying mechanism and in vivo biological performance remain unclear, which are essential for the clinical application of Ta-coated biomaterials as dental implants.

Purpose: The main objective of this study is to investigate the antibacterial activity of Ta-modified titanium (Ti) implants against peri-implantitis-related microbes and the potential molecular mechanisms.

Methods: *Fusobacterium nucleatum* and *Porphyromonas gingivalis* were selected to evaluate the antibacterial activity and potential antibacterial mechanism of Ta modification. The in vivo biocompatibility of Ta-modified implants was also evaluated.

Results: The results showed that Ta-modified surface performed excellent antimicrobial activity against *Fusobacterium nucleatum* and *Porphyromonas gingivalis*. Micro galvanic might be formed between the incorporated Ta and the Ti base, which could consume the protons and result in decreased ATP synthesis and increased ROS generation. The gene expression of bacterial virulence factors associated with cellular attachment, invasion and viability as the target of ROS was downregulated. Importantly, in vivo biological studies showed that Ta modification significantly promoted the osseointegration of implants by stimulating the expression of bone-forming proteins.

Conclusion: This study may provide some insights into clinical applications of Ta-coated Ti implants, especially in possibly infected situations.

Keywords: tantalum-coating, antibacterial activity, ATP synthesis, ROS generation, osseointegration

Introduction

Titanium (Ti) dental implants account for the majority of commercial implants market because of their excellent biocompatibility and load-bearing mechanical properties.[1] The clinical success of dental implants depends critically on the optimum and long-lasting osseointegration of the material. However, Ti implants, even those thoroughly sterilized, are prone to bacterial infections due to the compromised host defense and antibacterial properties of Ti.[2] Peri-implant infections caused by bacteria remain one of the most common and intractable problems for Ti implants, which would compromise the osseointegration and even result in implant shedding.[3,4] Thus, there is a practical need to improve the antibacterial activities of Ti implants.

Tantalum (Ta) has been considered a promising metallic material for biomedical implants or coatings in dental, orthopedic and arthroplasty applications due to its

Correspondence: Hong-Chang Lai; Jun-Yu Shi
Department of Implant Dentistry, National Clinical Research Center for Oral Diseases, Shanghai Key Laboratory of Stomatology, Shanghai Ninth People's Hospital, Shanghai Jiao Tong University School of Medicine, 500 Quxi Road, Shanghai 200011, People's Republic of China
Tel +86 21 23271699 (ext. 5298)
Fax +86 21 53073068
Email lhc9@hotmail.com; sakyamuni_jin@163.com

submit your manuscript | www.dovepress.com
DovePress
http://doi.org/10.2147/IJN.S218640

preferred anticorrosion, radiopacity, biocompatibility, osteogenic properties and antibacterial activities.[5,6] A retrospective case series of 966 patients showed a lower rate of re-infection in the revision cases using Ta acetabular components compared to those using Ti ones,[7] which suggested that Ta might have antibacterial properties to hinder biofilm formation. It has also been demonstrated that *S. aureus* adhesion was less likely to adhere to pure Ta than to Ti alloy.[8] Ta-based coatings encompassing TaO and TaN have an antimicrobial effect against oral pathogens in artificial saliva.[9,10] However, significant gaps still exist in the antimicrobial mechanism of Ta or Ta-based coatings. It is hypothesized that Ta modification could enhance the osseointegration of Ti dental implants and osteoblasts may win the race for the surface more easily compared with bacteria. It is also hypothesized that microorganisms would find it difficult to colonize the surface due to the surface chemistry of Ta or Ta-based coatings.

We have previously incorporated Ta into the Ti implants by magnetron sputtering and found that Ta_2O_5 coating with a micro/nano hierarchical structure was formed on Ti, which significantly enhanced the in vitro osteogenic activity of Ti implants.[11] The Ta_2O_5 coating could also promote selective adhesion of rat bone mesenchymal stem cells (rBMSCs) rather than oral pathogens in a co-culture model of cell and bacteria,[12] indicating that "osteoclasts win the race for Ta-modified surface rather than bacteria". However, a better understanding of the relationship between the physicochemical properties and the antibacterial effectiveness of Ta_2O_5 coating is still required. Although the enhanced osteogenic activity may partially account for the antibacterial property of Ta coating, it's also of great importance to investigate the antibacterial mechanism of Ta_2O_5 coating with hierarchical structure and whether Ta modification results in an improvement of osseointegration in vivo.

The aim of this study is to evaluate the antibacterial activity and the in vivo bioactivity of Ta-coated Ti implants. *Fusobacterium nucleatum* and *Porphyromonas gingivalis*, two of the most commonly suspected pathogens for peri-implant infections,[13] were used to evaluate the antibacterial activities of Ta-modified Ti implants (SLA-Ta) through live/dead fluorescent staining, colony-forming unit (CFU) counting method and scanning electron microscopy (SEM) technique. The antibacterial mechanism was investigated by measuring ATP synthesis, reactive oxygen species (ROS), lipid peroxidation (LPO), catalase (CAT) activity, glutathione (GSH) levels and gene transcriptional assays. The osseointegration of SLA-Ta implants was also evaluated using a canine implant model.

Materials And Methods

Preparation Of Materials

Commercial pure Ti discs (diameter: 15 mm, thickness: 1 mm) and Ti implants (diameter: 3.3 mm, length: 10 mm) of grade IV with SLA (sand-blasted, large-gritted, acid-etched) surfaces were prepared. Ta was implanted onto the SLA Ti disk by magnetron-sputtering technique as described in our previous study.[11] Simply, Ti base was firstly sputter-cleaned for 5 mins and sputtered with Ti for 10 mins. Then, Ta deposition was done for 40 mins by sputtering. The surface of Ta_2O_5 coating with a micro/nano hierarchical structure has been characterized in our previous study. The topography and the localized potential distribution of Ta-coated implants were examined by field emission-scan electron microscopy (FE-SEM) and atomic force microscope (AFM), respectively. All samples were sterilized using gamma radiation (25KGY) before use.

Antibacterial Performances

Bacterial culture: *Fusobacterium nucleatum* (*F. nucleatum*, ATCC 25586) and *Porphyromonas gingivalis* (*P. gingivalis*, ATCC33277) were cultured in the brain heart infusion (BHI) broth medium (Oxoid) supplemented with sheep blood under standard anaerobic conditions.

Fluorescence staining: After incubation with bacteria medium (10^7 CFU/mL for *F. nucleatum* and *P. gingivalis*) for 24hrs, the samples were stained with LIVE/DEAD BacLight Bacterial Viability Kits (Invitrogen) for 15mins in darkness, rinsed with PBS for 3 times and finally observed under the confocal laser scanning microscope (CLSM; Leica, Hamburg, Germany).

Spread plate method: After incubation with bacteria medium (the same concentration as above) for 24hrs, non-adhered bacteria were removed, and adhered bacteria were ultrasonically detached as previously described. The detached bacteria were diluted serially and cultivated on sheep blood agar plates for 48hrs (*F. nucleatum*) and 72hrs (*P. gingivalis*) in triplicate, respectively. CFUs were counted according to the National Standard of China GB/T 4789.2 protocol. Antibacterial rate (%) = (CFUs of SLA group – CFUs of SLA-Ta group)/CFUs of SLA group×100%.

SEM observation: After incubation with bacteria medium (the same concentration as above) for 24hrs, the

samples were fixed with 4% glutaraldehyde for 2hrs at 4°C after gentle rinsing with PBS. Then, a series of ethanol solutions were used to sequentially dehydrate all samples for 10 min each. The samples were dried, sputter-coated with platinum and then observed under SEM.

Antibacterial longevity and stability: The disks were soaked in PBS for up to 60 days to evaluate the long-term antibacterial activity. At selected time points (1, 30 and 60d), the samples were cultured with bacteria medium (the same concentration as above) for 24hrs and the antibacterial rates of the SLA-Ta surface were evaluated as above. Then, the samples were cleaned ultrasonically, re-sterilized and re-inoculated after incubation with bacteria medium for 24 h. The process was repeated for three times and the antibacterial rate was measured to assess the stability of antibacterial activity.

Antibacterial Mechanism

F-type ATPase activity and ATP levels: *P. gingivalis* and *F. nucleatum* in the logarithmic phase of growth were cultured on SLA-Ta surface for 24 h and then gathered by centrifugation at 6000 rpm for 5 min. *P. gingivalis* and *F. nucleatum* on the SLA surface were selected as the control group. Membrane proteins were extracted, and F-type ATPase activities of the gathered bacteria were measured by F-type ATPase activity assay kit (Genmed Scientifics Incorporated, China) in accordance with the instruction. ATP levels of the bacteria were measured by the ATP assay kit (Beyotime Institute of Biotechnology, China). The protein contents of the bacteria were detected using the BCA method in order to standardize all samples for comparison. The experiments were done in triplicate.

ROS Generation: ROS levels were measured using DCFH-DA. Non-fluorescent DCFH-DA could be oxidized to highly fluorescent 2′7′-dichlorofluorescin (DCF) by oxidants. *P. gingivalis* and *F. nucleatum* (the same concentration as above) were cultured on the sample discs for 24hrs. The bacteria co-cultured with discs were stained with 500 μL DCFH-DA (1.0×10^{-6} M) for 30 min at 37 °C. Then, the fluorescence intensities were measured at 488 nm excitation wavelength/535 nm emission wavelength by the microplate reader.

LPO levels: The LPO level was an indicator of cell membrane damage because of oxidative stress. The LPO levels of the bacteria cultured on two surfaces were measured by a lipid peroxidation assay kit according to the manufacturer's instructions (Nanjing Jiancheng Bioengineering Institute). The absorbance was measured at 532 nm by spectrophotometer (Thermo). The results were expressed as nmol/mg pro.

CAT Activity: CAT is a key antioxidant enzyme of microbial antioxidant system. The CAT activities of bacteria cultured on the samples were tested by CAT assay kit (Beyotime Institute of Biotechnology, China) according to the instruction of manufacturers. The absorbance was measured at 405 nm by the spectrophotometer (Thermo), and the CAT activity (U) was defined as the clearance of 1 μmol H_2O_2 every second and recorded as U/mL.

GSH Levels: GSH as a key component of the antioxidant system can protect cells from oxidative stress. The GSH levels of the collected bacteria were tested by GSH assay kit (Beyotime Institute of Biotechnology, China) following the protocols of the manufacturer. The absorbance was measured at 420 nm by a spectrophotometer (Thermo). The results were expressed as mg/mL.

Gene transcriptional assay: *P. gingivalis* and *F. nucleatum* in the exponential phase were cultured on two surfaces for 24hrs. Bacteria were collected by centrifugation, extracted into RNA by trizol reagent (Takara, Japan), and then reversed into cDNA by PrimeScript™ RT reagent Kit (Takara, Japan). Real-time PCR was conducted using SYBR® Premix Ex Taq™ (Takara, Japan) and *16S* rRNA was selected as the internal control gene. The primers of genes are shown in Table 1.

In Vivo Biological Evaluation

Animal preparation and surgical procedures: All animal experiments in this study were approved by the Animal Care and Experiment Committee of Shanghai Ninth People's Hospital. All procedures were conducted according to the guidelines of the committee. Three adult male beagle dogs (25–35 kg) were used, and two surgical procedures were conducted here. Before each surgery, dogs were given general (Ketamine, 10 mg/kg, intramuscularly) and local anesthesia (40 mg of procaine and 0.05 mg of adrenaline). All premolars and first molars of the mandible were extracted bilaterally and penicillin (800,000 U/day) was given for 3 days. It took 3 months for the alveolar ridge to heal. During the second surgery, a mid-crestal incision was made and full-thickness periosteal flaps were elevated in the extraction area. Four sites were selected on each side of the mandibular bone and allocated to either SLA or SLA-Ta group. A total of 24 implantation sites were obtained with 12 sites for each group. The implantation sites were prepared by pilot (Ø 2.2 mm) and twist (Ø 2.8 mm) drills. All implants (Ø 3.3 mm and

Table 1 Primers Of The Target Genes

Gene	Primer sequence (5′→3′)	
	Forward	**Reverse**
P. gingivalis		
16S rRNA	TGTAGATGACTGATGGTGAAA	ACTGTTAGCAACTACCGATGT
hagA	ACAGCATCAGCCGATATTCC	CGAATTCATTGCCACCTTCT
hagB	TGTCGCACGGCAAATATCGCTAAAC	CTGGCTGTCCTCGTCGAAAGCATAC
rgpA	GCCGAGATTGTTCTTGAAGC	AGGAGCAGCAATTGCAAAG
rgpB	CGCTGATGAAACGAACTTGA	CTTCGAATACCATGCGGTT
kgp	AGCTGACAAAGGTGGAGACCAAAGG	TGTGGCATGAGTTTTTCGGAACCGT
F. nucleatum		
16S rRNA	AAGCGCGTCTAGGTGGTTATGT	TGTAGTTCCGCTTACCTCTCCAG
fadA	CACAAGCTGACGCTGCTAGA	TTACCAGCTCTTAAAGCTTG
dnak	GTATCCCTGCTGCTCCAA	GTGCTTCTGCTTCCTTAGTC
groEL	ATTGACCCAGCAAAAGTTAC	GGCATCATTCCACCAGCA
tnaA	TGAACAAAGGGAACGTGCATT	ATTCCAGCAGGGAAAGCAAA

10 mm in length) were inserted. The machined neck of the implant was located at the buccal margin level and all implants were attached with Ti healing caps. The wound was closed without stress and the implants were left to heal unsubmerged. Four weeks later, dogs were sacrificed, and their mandibles were dissected into eight parts according to the implants. Each sample with one implant was fixed in 10% formalin solution (pH 7) for subsequent tests.

Micro-CT assay: Micro-CT (GE explore Locus SP Micro-CT; USA) was used to do the structural analysis of the fixed samples. A 1-mm region around the implant was selected and reconstructed. The ratio of bone volume to tissue volume (BV/TV), bone mineral density (BMD), trabecular thickness (Tb.Th) and trabecular number (Tb.N) of the bone in this region were analyzed.

Histomorphometric analysis: Samples were dehydrated in a series of alcohols from 75% to 100% and embedded in polymethylmethacrylate (PMMA). After that, they were cut into 150 mm thick sections using a Leica SP1600 saw microtome (Leica, Hamburg, Germany). All sections were glued to glass sides and then ground and polished to a thickness of 30 μm. Samples were stained with van Gieson's picrofuchsin for histological observation. The digital images were captured by a light microscope (CX21, Olympus, Tokyo, Japan). Histomorphometric measurements were performed by Image-Pro plus 6.0 (Media Cybernetics Inc., Silver Spring, MD, USA). BIC (%) was defined as the length of the bone-to-implant contact or the length of the implant surface;, and the bone density within the threads (BDWT, %) was defined as the percentage of the mineralized area in the adjacent bone within the implant threads.

Immunohistochemical analysis: The fixed sample was cut into two sections along the long axis of the implant by a microtome, and both of them were placed in liquid nitrogen for several minutes and then taken out for 3–4 times until the integrated bone was separated from the implants without pressure. The integrated bone was decalcified, dehydrated, fixed in paraffin and then cut into buccal-lingual serial slices (approximately 5 μm). After deparaffinization and rehydration, antigen unmasking was performed by heating slices in retrieval solution in a 90° C water bath for 20 min. The endogenous peroxidase activity was quenched with 3% hydrogen peroxide at room temperature for 25 min in dark. After washing with PBS (pH 7.4) three times, nonspecific sites were blocked with BSA for 30 min. Slices were incubated with the primary mouse monoclonal antibody to OCN or COL1 (1:100 dilution, Abcam, USA) in a humidified chamber at 4° C overnight. After washing with PBS, slices were incubated with secondary anti-mouse antibody (horseradish peroxidase marked) for 50 mins. After washing with PBS, DAB solution was added dropwise and the antibody–antigen complexes were stained brownish yellow. Nuclei were counterstained with Harris hematoxylin for about 1 min, and slices were dehydrated and sealed with neutral gum. The digital images were taken by a light microscope (CX21, Olympus, Tokyo, Japan). The results were interpreted as follows: (1) Positive areas: all integrated bone tissues were positively stained and considered as 100%; (2) Staining intensity: (+) light-yellow; (++)

yellow-brown; (+++) dark-brown. So, the strengths indicate"+" "'++'" and "'+++'" in Figure 9 are the staining intensity here.

Statistical Analysis

All experiments were conducted in triplicate. The data were shown as mean ± standard deviation. Statistical comparisons were performed using Graph-Pad Prism statistical software package. The differences were tested using Student's *t*-test (two groups) and $P< 0.05$ was considered statistically significant.

Results

Topography Of Ta-Coated Implants

At low magnification, micro pits were observed on the surface of SLA Ti implants (Figure 1A). However, Ta coating resulted in the distribution of Ta with nano-structure in the micro pits of SLA and an increase in the roughness of Ta-coated implants, thus forming a hierarchical nano-micro structure (Figure 1B). The localized potential distribution of both surfaces was scanned and measured using AFM. The Volta potential difference of SLA-Ta surface was more positive than that of SLA surface, indicating that a galvanic couple might be formed on SLA-Ta surface.

Antibacterial Activities

Antibacterial Activities Of The SLA-Ta Surface

Gram-negative *P. gingivalis* and *F. nucleatum* have been shown to be involved in peri-implant infections. Therefore, the antimicrobial activities of the SLA-Ta surface against these two bacteria were evaluated at 24 h by live/dead staining, CFU counting method and SEM observation. Living and dead bacteria on two samples were visualized by live/dead staining. All bacteria, regardless of whether they had intact or damaged membranes, could be stained green; while only those bacteria with damaged membranes were stained red. Both *P. gingivalis* and *F. nucleatum* were less likely to adhere to the SLA-Ta surface than to the SLA surface (Figure 2A). The majority of bacteria adhered to the SLA surface were stained green, whereas more bacteria stained red were found on the SLA-Ta surface, thus indicating that SLA-Ta had higher antibacterial activity than SLA.

As shown in Figure 2B, more viable *P. gingivalis* and *F. nucleatum were* detached from the SLA surface compared to that from the SLA-Ta surface, demonstrating that the SLA-Ta surface could reduce the viability of pathogenic bacteria. Notably, the antibacterial rate of SLA-Ta against *P. gingivalis* and *F. nucleatum* was approximately 51% and 64%, respectively.

Figure 2C shows the morphology of *P. gingivalis* and *F. nucleatum* cultured on different surfaces for 24 h. More bacteria with intact cell membranes undergoing the binary or multiple fission processes were detected on the SLA surface. The biofilm formed on the SLA surface was composed of bacteria and secreted extracellular polymeric substances (EPS), especially in *P. gingivalis*. However, less bacteria without EPS were observed on the SLA-Ta surface.

Antibacterial Longevity And Stability Of SLA-Ta Surface

As shown in Figure 3A, the antibacterial rate of SLA-Ta against *P. gingivalis* and *F. nucleatum* remained at around 50% and 60%, respectively. Incubation in PBS for up to 60 days resulted in no significant changes in the antibacterial rate of the SLA-Ta surface, indicating long-term antibacterial activity of the SLA-Ta surface. Similar results were also found after three cycles of bacteria attack (Figure 3B), suggesting high antibacterial stability of the SLA-Ta surface.

Antibacterial Mechanism Of SLA-Ta Surface

ATP Synthesis

The membrane proteins of *P. gingivalis* and *F. nucleatum* on SLA and SLA-Ta surfaces were extracted and the F-type ATP synthase activity was determined. It showed that the F-type ATP synthase activity of *P. gingivalis* and *F. nucleatum* on the SLA-Ta surface was significantly decreased (Figure 4A and C). The F-type ATP synthase is the main enzyme of ATP synthesis and its activity is positively related to the ATP level. As expected, the ATP level was also significantly decreased in *P. gingivalis* and *F. nucleatum* on the SLA-Ta surface (Figure 4B and D).

ROS Generation

The generation of ROS by bacteria co-cultured with SLA or SLA-Ta samples was determined by measuring the fluorescence intensity of 2′7′-dichlorofluorescin (DCF) probe. The fluorescence intensities of *P. gingivalis* and *F. nucleatum* as an indicator of free radical formation were significantly increased in the SLA-Ta group (Figure 5A). The LPO level as a reliable indicator of cell membrane damage as a

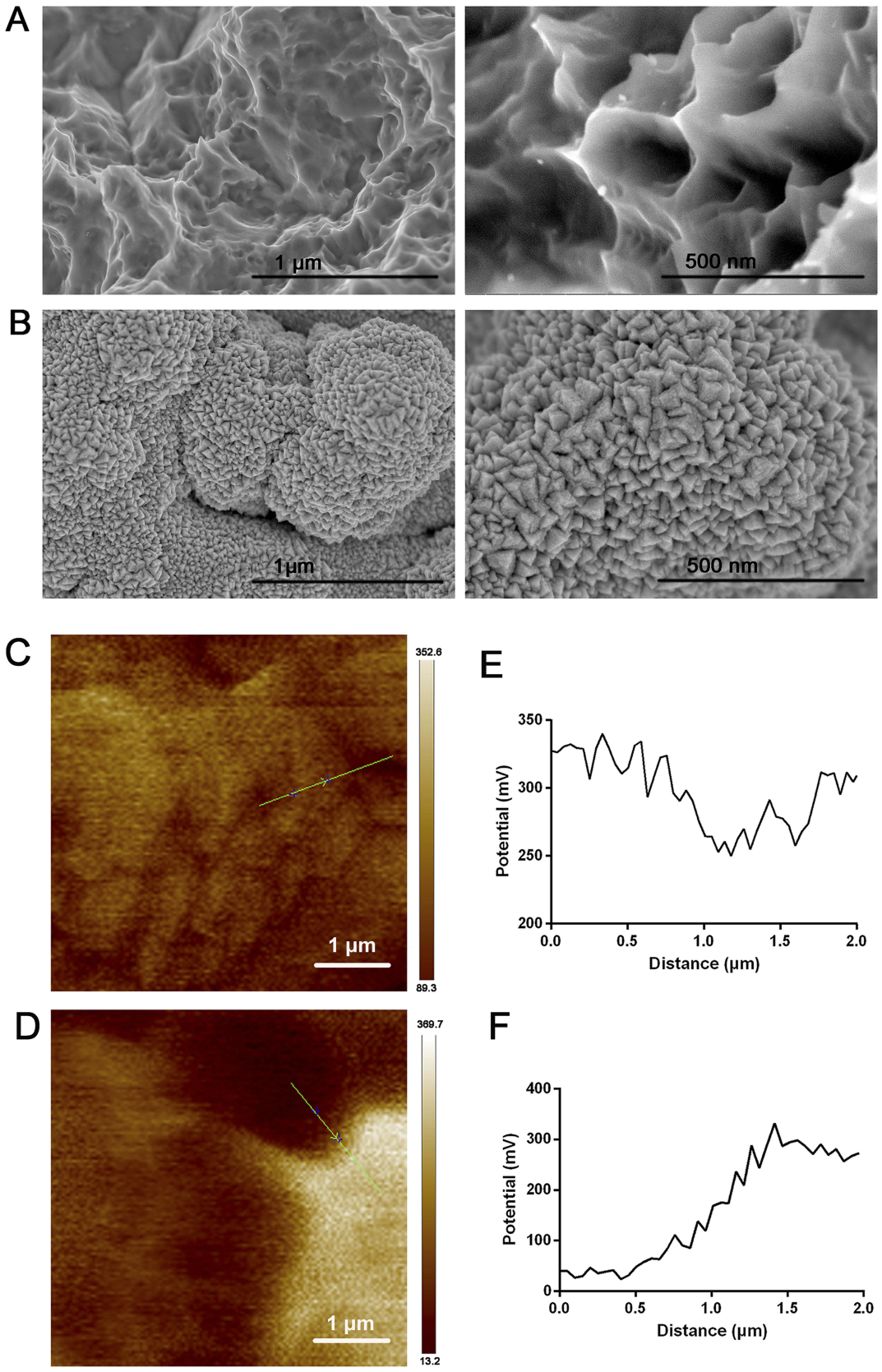

Figure 1 FE-SEM scanning of SLA (**A**) and Ta-coated implant (**B**), in which the left part indicated the low magnification and the right part indicated the high magnification. Surface voltage potential mapping of SLA (**C**) and Ta-coated implant (**D**) scanned by AFM. The analysis of relative voltage potential (green line in C and D) on SLA (**E**) and Ta-coated surface (**F**).

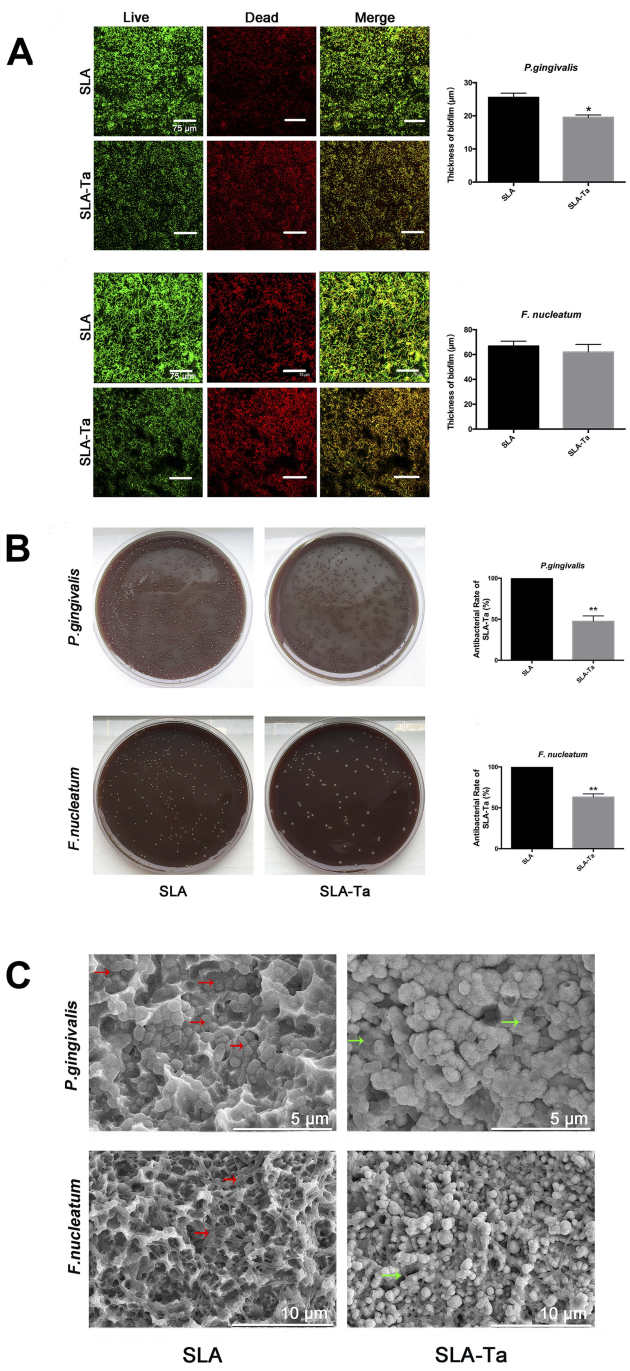

Figure 2 (**A**) Fluorescent images and the biofilm thickness of *P. gingivalis* and *F. nucleatum* cultured on SLA and SLA-Ta surfaces for 24 h, obtained by CLSM after live/dead staining. (**B**) Re-cultivated bacterial colonies of *P. gingivalis* and *F. nucleatum* (detached from SLA and SLA-Ta) on agar plate. The antibacterial rate of SLA-Ta surface against *P. gingivalis* and *F. nucleatum* was also calculated. (**C**) SEM morphologies of *P. gingivalis* and *F. nucleatum* seeded on SLA and SLA-Ta at 24hrs, the red arrow represented the EPS formed by the bacteria on SLA surface and the green arrow represented the crinkled bacteria on SLA-Ta surface.
Abbreviation: EPS, extracellular polymeric substances.

consequence of oxidative stress was also measured in *P. gingivalis* and *F. nucleatum* co-cultured with SLA or SLA-Ta samples, and the results were consistent with those of ROS generation (Figure 5B). The GSH and CAT activities were significantly reduced in the SLA-Ta group at 24 h compared to the SLA control group (Figure 5C and D), suggesting that incorporation of Ta could promote the oxidative stress of bacteria.

Gene Expression

Changes in the virulence of bacteria in the exponential phase were evaluated by Real-time PCR. Both *P. gingivalis* and *F. nucleatum* were cultured on SLA and SLA-Ta surfaces for 24 h, and the expression of genes related to bacterial attachment and biofilm formation was determined. As shown in Figure 6A, Ta incorporation significantly downregulated the expression of genes such as *hagA/B*, *kgpA/B* and *kgp* in *P. gingivalis*. Meanwhile, the expression levels of *fadA*, *dnaK* and *groEL* in *F. nucleatum* cocultured with SLA-Ta samples were decreased significantly at 24 h compared to the SLA group (Figure 6B). Thus, Ta incorporation could inhibit the expression of genes related to bacterial attachment and biofilm formation and thus resulted in changes in bacterial virulence.

Biological Evaluation Of Ta-Coated Implants

Micro-CT Analysis

The reconstructed micro-CT 3D images of the two groups were shown in Figure 7A, where the implant was marked in yellow and the bone around the implant was marked in white. Figure 7B–E clearly showed that bone volume, BMD, BV/TV, Tb.Th and Tb.n were significantly higher in the SLA-Ta group than in the SLA group ($P<0.05$).

Histological Analysis

The in vivo osseointegration in histological sections stained with Van Gieson's picrofuchsin staining was shown in Figure 8A. In line with the micro-CT analysis, more corticocancellous bone was obtained in the SLA-Ta group, indicating better osseointegration of the Ta coating. Cervical osseointegration was highly associated with the initial stability of the implants and thus had important effects on the success rate of dental implantation. The results showed that Ta modification obviously promoted cervical osseointegration. Figure 8B shows that the BIC of Ta-coated implants (around 44.3%) was significantly higher than that of Ta-modified ones (around 35.6%, $p < 0.05$). A similar phenomenon was also observed for the percentage of BDWT (Figure 8C).

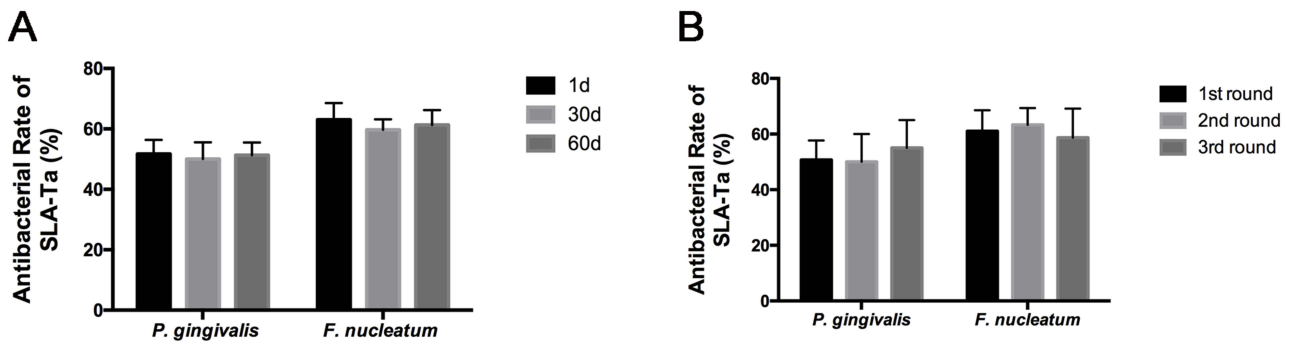

Figure 3 Antibacterial rates of the SLA-Ta surface after incubation with PBS for 1, 30, and 60 days (**A**) and repeated bacterial attack (**B**).

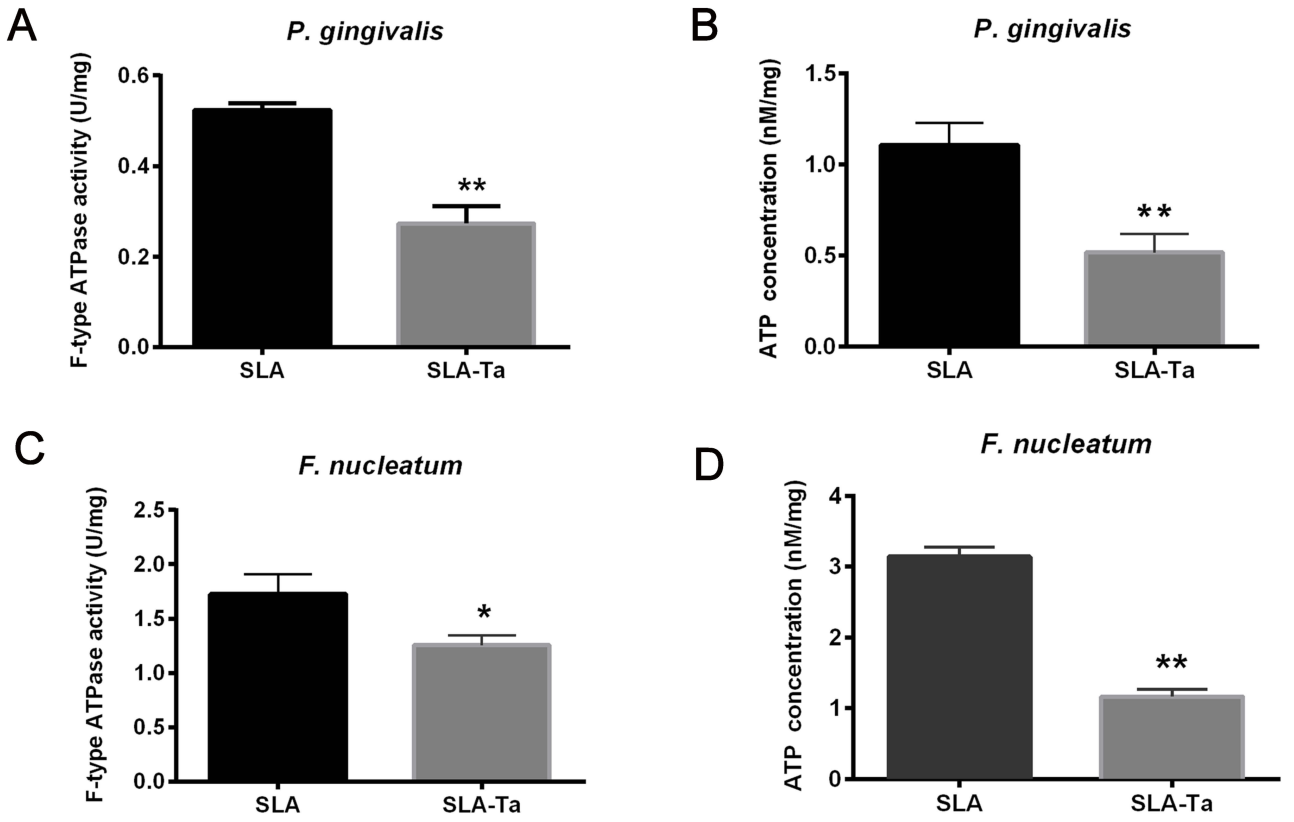

Figure 4 F-type ATP synthase activity of *P. gingivalis* (**A**) and *F. nucleatum* (**C**) cultured on SLA and SLA-Ta surfaces for 24hrs. ATP levels of *P. gingivalis* (**B**) and *F. nucleatum* (**D**) cultured on SLA and SLA-Ta surfaces for 24hrs. *P<0.5, significantly different from the control SLA group. **P<0.01, significantly different from the control SLA group.

Immunohistochemical Analysis

The osteogenic proteins, including COL1 and OCN which were closely related to osseointegration, at the bone interface adjacent to SLA and SLA-Ta implant surfaces were immunostained at 4 weeks. Although the intensity of COL1 antigen reactivity was increased in both groups, the COL1 reactivity appeared to be much stronger in the bone of SLA-Ta surface. Similarly, OCN staining was more pronounced in the bone of Ta-coated surface (Figure 9).

Discussion

Ta-based coatings can not only enhance the osteogenic differentiation in vitro, but they can also exhibit excellent antimicrobial properties.[14] Nevertheless, their antimicrobial activity against oral peri-implantitis related pathogens and the underlying mechanism remain poorly understood. Therefore, the antibacterial activity of previously established Ta_2O_5 coating (SLA-Ta surface) against two suspected peri-implant pathogens was investigated in this study.

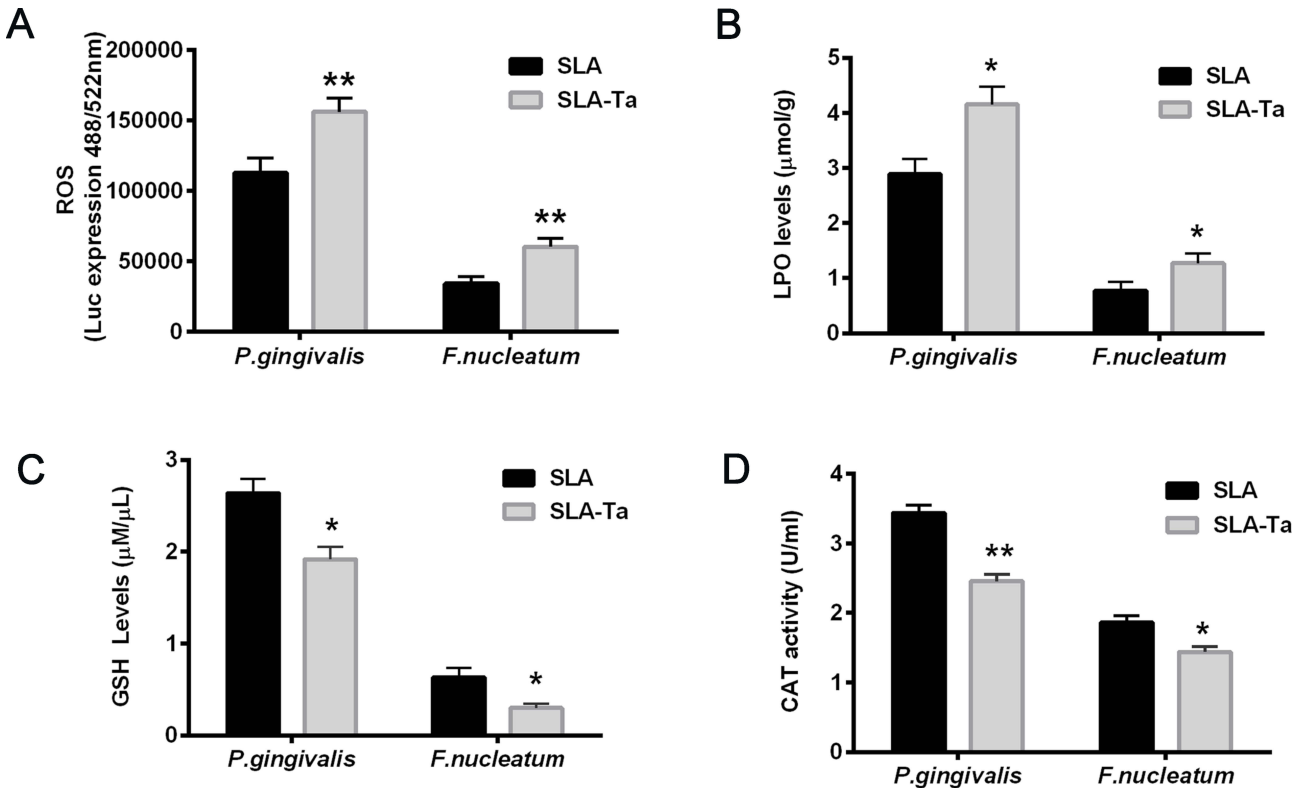

Figure 5 The fluorescence intensities of ROS (**A**), LPO levels (**B**), GSH levels (**C**) and CAT activities (**D**) of *P. gingivalis* and *F. nucleatum* co-cultured with SLA/SLA-Ta samples for 24hrs. *P<0.5, significantly different from the control SLA group. **P<0.01, significantly different from the control SLA group.
Abbreviations: ROS, reactive oxygen species; LPO, lipid peroxidation; GSH, glutathione, CAT-catalase.

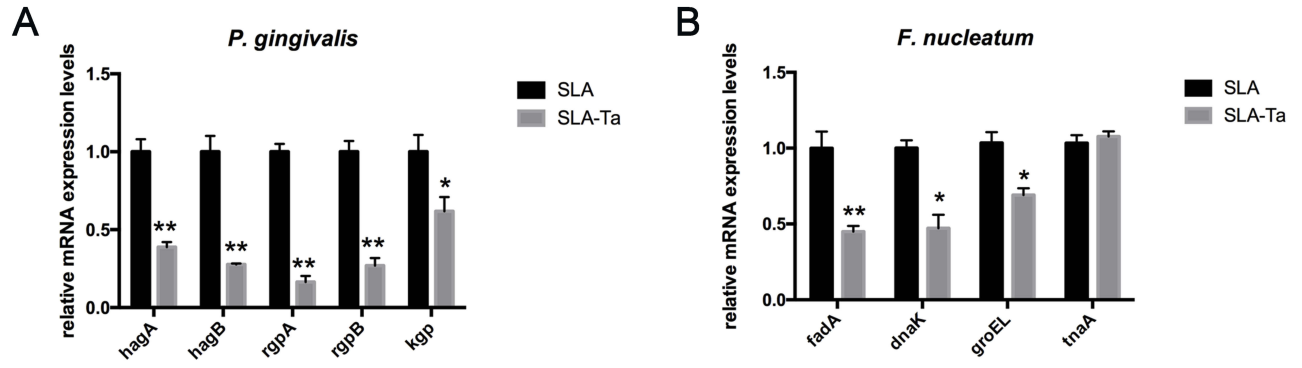

Figure 6 The expression of genes related to bacterial attachment and biofilm formation was determined by RT-PCR. Gene expression of *P. gingivalis* (**A**) and *F. nucleatum* (**B**) after incubation with both samples for 24hrs. *P<0.5, significantly different from the control SLA group. **P<0.01, significantly different from the control SLA group.

Many gram-negative anaerobic bacteria such as *P. gingivalis* and *F. nucleatum* have been found around failing implants.[13,15] It is noted that the implant surface is particularly susceptible to bacterial colonization in the first day of implantation.[16] In the present study, Figure 2 shows that the viability of pathogenic microbes on the SLA-Ta surface was effectively inhibited in the first day. The cell membranes of *P. gingivalis* and *F. nucleatum* on the SLA-Ta surface were more likely to be damaged, and the SLA-Ta surface also hampered the biofilm formation of *P. gingivalis* with a decreased thickness (Figure 2A). The total number of adherent bacteria on the SLA-Ta surface was also decreased, which was consistent with the assay of re-cultivated bacterial colonies (Figure 2B). The biofilm formed on the SLA-Ta surface was composed of more wrinkled bacteria without EPS (Figure 2C), which could contribute to the bio-corrosion of metallic materials but made it difficult for the eradication of bacteria in biofilms.[9]

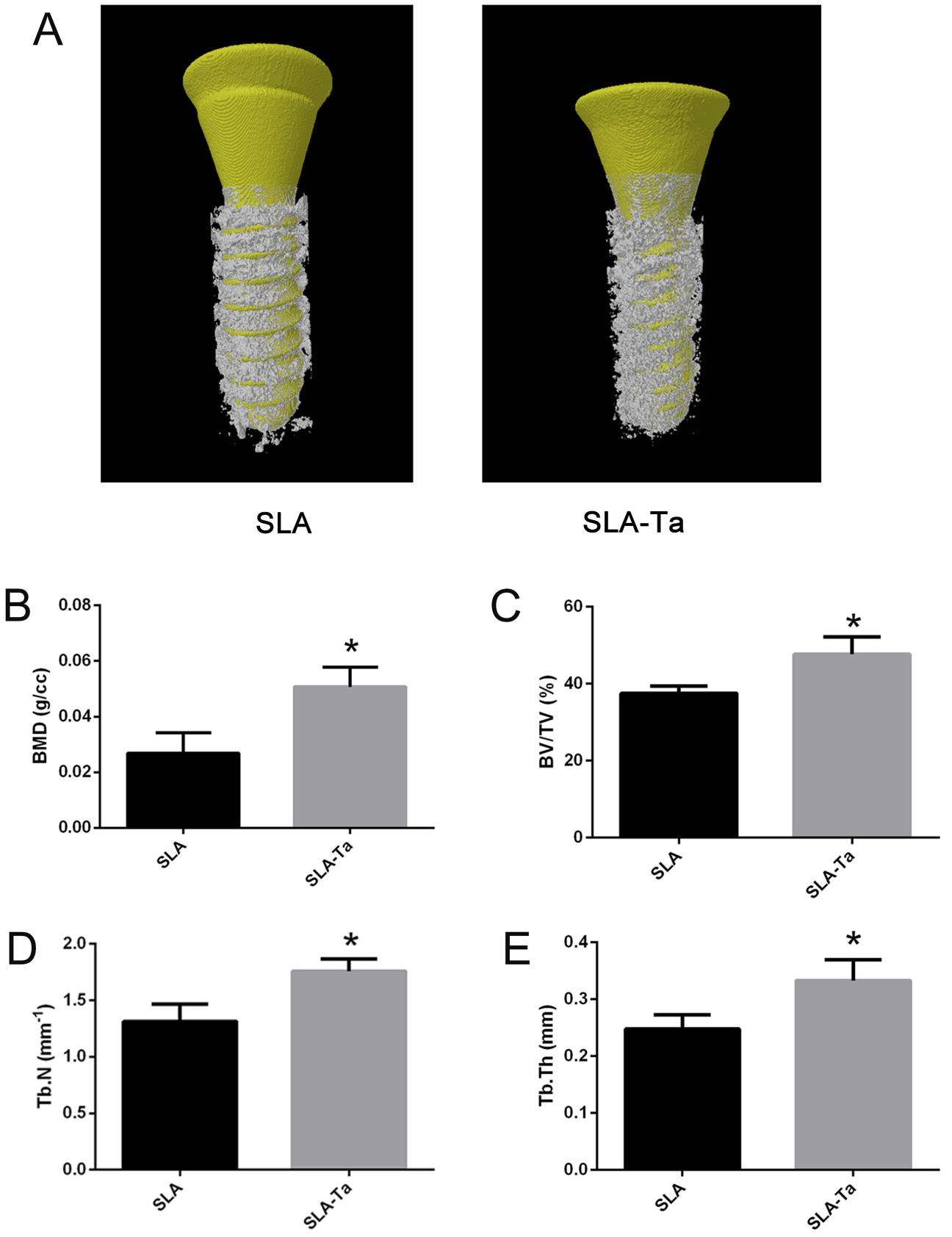

Figure 7 Micro-CT evaluation of bone tissue around dental implants at 4 weeks after implantation. (**A**) The reconstructed images of the implants and the surrounding bone in two groups; the BMD (**B**), BV/TV (**C**), Tb.N (**D**) and Tb.Th (**E**) of the bone adjacent to the implant surface were quantified, *P<0.5, significantly different from the control SLA group.

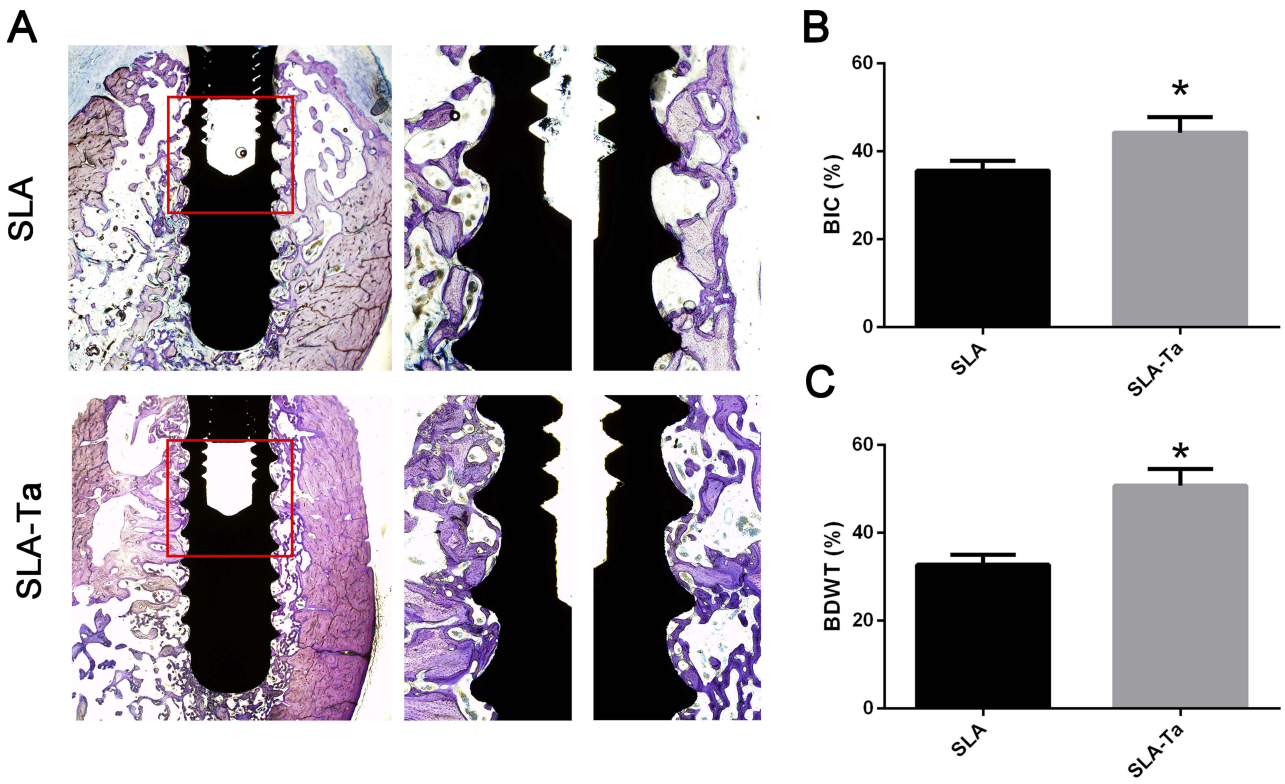

Figure 8 Ta-modification-enhanced bone osseointegration at 4 weeks. (**A**) After implantation for 4 weeks, the undecalcified sections were stained with van Gieson's. The BIC (B) and BDWT (C) of the bone adjacent to the implant surface in ROI. The area of interest (ROI, the red rectangle area of A) was for the analysis of BIC and BDWT. *P<0.5, significantly different from the control SLA group.

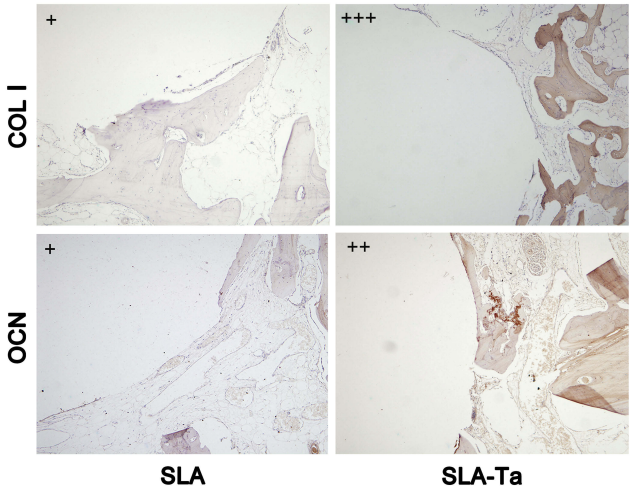

Figure 9 The immunochemical staining of COLI and OCN in the integrated bone tissue of two groups at 4 weeks. Relative strength index of the staining; (+) light-yellow; (++) yellow-brown; (+++) dark-brown.

Microbial infections may occur peri-operatively or over the lifetime of the implant.[16] However, immersion in PBS for 60 days or repeated bacterial attack resulted in no significant changes in the antibacterial rate of the SLA-Ta surface (Figure 3). It was noteworthy that the bacterial suspension here was much harsher than that in in vivo situations, indicating that SLA-Ta would have long-term stable antibacterial activity.

The mechanism of the improved antibacterial activity of the SLA-Ta surface remains unknown. One possible mechanism might be the micro-galvanic couples generated between the incorporated Ta and the Ti base (Figure 1C), which could lead to cathodic consumption of protons and anodic release of Ta.[17–20] Various metallic ions such as Ag and Zn have been incorporated into the Ti base, forming Ag/Ti or Ag/Zn galvanic couples.[17–19] Since the transmembrane proton electrochemical potential provides the driving force for ATP synthase, proton consumption resulted from Ta/Ti galvanic could damage the transmembrane proton gradient and interfere with ATP synthesis.[21] In our study, the F-type ATPase activity and ATP synthesis were decreased for both bacteria in the SLA-Ta group (Figure 4), which could further affect cell metabolism and even cause cell death.

ROS generation is a widely accepted mechanism for nanoparticle-induced bacterial toxicity.[22,23] The excessive generation of ROS encompassing •OH, H_2O_2 and O_2^- can

act on cell membranes, resulting in oxidative stress and imbalance of intracellular homeostasis and, consequently, disruption of cellular metabolism and even cell death.[24] In general, ROS is generated under aerobic conditions. Previous studies have shown that the electron holes on the surface of nanoparticles could react with oxygen and water to form O_2^- and •OH, respectively.[25] However, H_2O_2 and •OH could also be generated by the reaction of electron holes with water under anaerobic conditions.[26,27] The electron transfer between incorporated Ag nanoparticles and Ti base could induce ROS production and thus cause bacterial death.[20] *P. gingivalis* and *F. nucleatum* are obligate anaerobes, and thus the incorporation of Ta with a nanostructure may generate ROS through electron transfer and then affect bacterial cellular metabolism. The ROS level was found to be increased by the SLA-Ta surface (Figure 5A), and the LPO level which could damage cell membranes and decrease their fluidity was increased (Figure 5B).[28] It could be concluded that the elevated ROS level was associated with the disruption of the bacterial cellular structure as well as the antibacterial phenomenon. In living cells, there is always a homeostatic balance between ROS generation and elimination. CAT and GSH, two potent enzymatic scavengers of ROS, can protect cells against oxidative stress and maintain ROS at certain levels.[29,30] Our results showed that the SLA-Ta surface significantly decreased CAT and GSH activities (Figure 5C and D), indicating an increase in ROS generation. The stronger the antioxidant system, the higher the tolerance of a microorganism to the oxidative stress. Our results showed that the SLA-Ta surface had a stronger antibacterial effect on *F. nucleatum* than on *P. gingivalis*, possibly because *P. gingivalis* showed some tolerance to oxygen and thus was more resistant to ROS than *F. nucleatum*.

The inhibition of ATP synthesis and ROS generation can have an effect not only on the synthesis of cellular proteins and membrane lipids, but also on the virulence genes. The gene expression of bacterial virulence factors was shown in Figure 6. In *P. gingivalis*, *hagA* and *hagB* encoded proteins involved in bacterial colonization;[31] while *rgpA*, *rgpB* and *kgp* encoded proteases involved in bacterial motility and tissue destruction.[32] The down-regulation of these genes by the SLA-Ta surface could further lead to decreased expression of related proteins and consequently improved antibacterial effects, which was consistent with less EPS generation and thinner biofilm of *P. gingivalis* on the SLA-Ta surface. For *F. nucleatum*, the expression of *fadA* is related to bacterial adhesion and invasion;[33] and that of *dnak* and *groEL* plays an essential role in protecting *F. nucleatum* against various stress conditions including oxidative stress.[34] These gene transcriptional profiles were significantly down-regulated by the SLA-Ta surface, suggesting that the antimicrobial activity of the SLA-Ta surface against *F. nucleatum* was induced at a gene level. However, the SLA-Ta surface had no effect on the expression of *tnaA* which could enhance biofilm formation of *F. nucleatum*.[35] This was also in accordance with the results of biofilm formation of *F. nucleatum*.

During the initial step of osseointegration, bone marrow stem cells or osteoblasts would compete with the bacteria of oral cavity on the implant surface.[36] Both types of implants were inserted in the mandible alveolar bone of dogs and evaluated in vivo, and better osseointegration was achieved for Ta-modified implants. The micro-CT analysis proved that more bone was formed on the SLA-Ta surface than on the SLA surface (Figure 7). The histological analysis further confirmed that the new bone in direct contact with the SLA-Ta surface had higher BIC and BDWT (Figure 8).[37] Osseointegration might be enhanced due to the higher COL1 and OCN expression in the SLA-Ta group (Figure 9).[11,38] The in vivo evaluation showed that the Ta coating had excellent biocompatibility, and enhanced osseointegration that might make it easier for osteoblasts to win the race against bacteria.

The antibacterial mechanism of the SLA-Ta surface is elucidated in Figure 10. The micro galvanic formed by the SLA-Ta surface can reduce the transmembrane proton motive force, resulting in a decrease of ATP synthesis. Simultaneously, the ROS generated by Ta with a nanostructure promotes lipid peroxidation of cell membranes, enters bacterial cells and causes stress to cellular

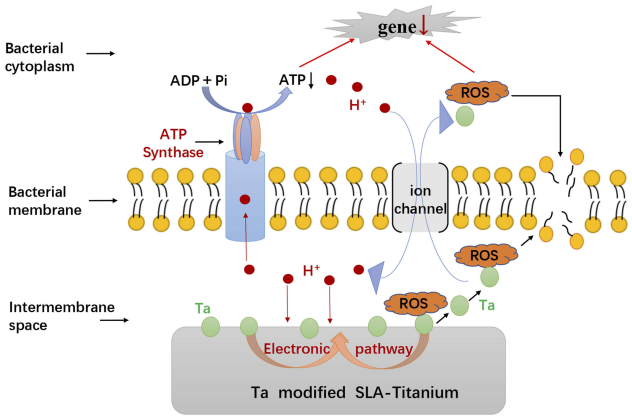

Figure 10 The schematic diagram of the possible antibacterial mechanism underlying the antimicrobial activity phenomenon of SLA-Ta surface.

metabolism. The inhibition of ATP synthesis and excessive ROS generation cause down-regulation of gene expression of bacterial virulence factors associated with cellular attachment, invasion and viability. Our study has also confirmed that the incorporation of Ta can enhance the osseointegration of the SLA surface. The SLA-Ta surface outperforms the traditional Ti-based SLA surface in improving osseointegration and maintaining sustainable antimicrobial activity against peri-implantitis related pathogens, which may be a new promising material for dental implants even in possibly infected clinical situations.

Conclusions

The SLA-Ta surface showed excellent antibacterial activity against *P. gingivalis* and *F. nucleatum* involved in peri-implant infections such as peri-implantitis. The SLA-Ta surface inhibited ATP synthesis and promoted ROS generation, resulting in lipid peroxidation of cell membranes and a decrease of CAT activity and GSH levels, and eventually disruption of cellular metabolism. The expression of bacterial virulence factors associated with cellular attachment and viability was down-regulated, which partly explained the antimicrobial activity of the SLA-Ta surface. The inhibition of ATP synthesis and the promotion of ROS generation might be ascribed to the micro galvanic and the electron transfer formed by SLA-Ta surface. The superior in vivo osseointegration of the Ta coating also partly accounts for its high antibacterial activity. The underlying antibacterial mechanism of the SLA-Ta surface proposed in this study may provide some insights into clinical applications of Ta-coated materials as dental implants, especially in the possibly infected clinical situations.

Acknowledgments

This work was sponsored by Shanghai sailing program (19YF1425900), National Natural Science Foundation of China (81771116) and Shanghai Summit & Plateau Disciplines.

Disclosure

The authors report no conflicts of interest in this work.

References

1. Spriano S, Yamaguchi S, Baino F, Ferraris S. A critical review of multifunctional titanium surfaces: new frontiers for improving osseointegration and host response, avoiding bacteria contamination. *Acta Biomater*. 2018;79:1–22. doi:10.1016/j.actbio.2018.08.013
2. Charalampakis G, Leonhardt A, Rabe P, Dahlen G. Clinical and microbiological characteristics of peri-implantitis cases: a retrospective multicentre study. *Clin Oral Implants Res*. 2012;23(9):1045–1054. doi:10.1111/j.1600-0501.2011.02258.x
3. Buser D, Janner SF, Wittneben JG, Bragger U, Ramseier CA, Salvi GE. 10-year survival and success rates of 511 titanium implants with a sandblasted and acid-etched surface: a retrospective study in 303 partially edentulous patients. *Clin Implant Dent Relat Res*. 2012;14(6):839–851. doi:10.1111/j.1708-8208.2012.00456.x
4. Zhao L, Chu PK, Zhang Y, Wu Z. Antibacterial coatings on titanium implants. *J Biomed Mater Res B Appl Biomater*. 2009;91(1):470–480. doi:10.1002/jbm.b.31463
5. Balla VK, Bodhak S, Bose S, Bandyopadhyay A. Porous tantalum structures for bone implants: fabrication, mechanical and in vitro biological properties. *Acta Biomater*. 2010;6(8):3349–3359. doi:10.1016/j.actbio.2010.01.046
6. Lu T, Wen J, Qian S, et al. Enhanced osteointegration on tantalum-implanted polyetheretherketone surface with bone-like elastic modulus. *Biomaterials*. 2015;51:173–183. doi:10.1016/j.biomaterials.2015.02.018
7. Tokarski AT, Novack TA, Parvizi J. Is tantalum protective against infection in revision total hip arthroplasty? *Bone Joint J*. 2015;97-B(1):45–49. doi:10.1302/0301-620X.97B1.34236
8. Schildhauer TA, Robie B, Muhr G, Koller M. Bacterial adherence to tantalum versus commonly used orthopedic metallic implant materials. *J Orthop Trauma*. 2006;20(7):476–484. doi:10.1097/00005131-200608000-00005
9. Zhang Y, Zheng Y, Li Y, et al. Tantalum nitride-decorated titanium with enhanced resistance to microbiologically induced corrosion and mechanical property for dental application. *PLoS One*. 2015;10(6):e0130774. doi:10.1371/journal.pone.0130774
10. Maho A, Linden S, Arnould C, Detriche S, Delhalle J, Mekhalif Z. Tantalum oxide/carbon nanotubes composite coatings on titanium, and their functionalization with organophosphonic molecular films: a high quality scaffold for hydroxyapatite growth. *J Colloid Interface Sci*. 2012;371(1):150–158. doi:10.1016/j.jcis.2011.12.066
11. Shi J, Zhang X, Qiao S, et al. Enhanced osteointegration of tantalum-modified titanium implants with micro/nano-topography. *RSC Adv*. 2017;7(73):46472–46479. doi:10.1039/C7RA08036K
12. Zhu Y, Gu Y, Qiao S, Zhou L, Shi J, Lai H. Bacterial and mammalian cells adhesion to tantalum-decorated micro-/nano-structured titanium. *J Biomed Mater Res A*. 2017;105(3):871–878. doi:10.1002/jbm.a.35953
13. Zhuang LF, Watt RM, Mattheos N, Si MS, Lai HC, Lang NP. Periodontal and peri-implant microbiota in patients with healthy and inflamed periodontal and peri-implant tissues. *Clin Oral Implants Res*. 2016;27(1):13–21. doi:10.1111/clr.12508
14. Li X, Wang L, Yu X, et al. Tantalum coating on porous Ti6Al4V scaffold using chemical vapor deposition and preliminary biological evaluation. *Mater Sci Eng C Mater Biol Appl*. 2013;33(5):2987–2994. doi:10.1016/j.msec.2013.03.027
15. Albertini M, Lopez-Cerero L, O'Sullivan MG, et al. Assessment of periodontal and opportunistic flora in patients with peri-implantitis. *Clin Oral Implants Res*. 2015;26(8):937–941. doi:10.1111/clr.12387
16. Pritchard EM, Valentin T, Panilaitis B, Omenetto F, Kaplan DL. Antibiotic-releasing silk biomaterials for infection prevention and treatment. *Adv Funct Mater*. 2013;23(7):854–861. doi:10.1002/adfm.201201636
17. Jin G, Qin H, Cao H, et al. Synergistic effects of dual Zn/Ag ion implantation in osteogenic activity and antibacterial ability of titanium. *Biomaterials*. 2014;35(27):7699–7713. doi:10.1016/j.biomaterials.2014.05.074
18. Cao H, Tang K, Liu X. Bifunctional galvanics mediated selective toxicity on titanium. *Mater Horiz*. 2018;5(2):264–267. doi:10.1039/C7MH00884H

19. Wang S, Wu J, Yang H, Liu X, Huang Q, Lu Z. Antibacterial activity and mechanism of Ag/ZnO nanocomposite against anaerobic oral pathogen Streptococcus mutans. *J Mater Sci Mater Med*. 2017;28(1):23. doi:10.1007/s10856-016-5837-8
20. Wang G, Jin W, Qasim AM, et al. Antibacterial effects of titanium embedded with silver nanoparticles based on electron-transfer-induced reactive oxygen species. *Biomaterials*. 2017;124:25–34. doi:10.1016/j.biomaterials.2017.01.028
21. Zharova TV, Vinogradov AD. Energy-dependent transformation of F0.F1-ATPase in *Paracoccus denitrificans* plasma membranes. *J Biol Chem*. 2004;279(13):12319–12324. doi:10.1074/jbc.M311397200
22. Ruparelia JP, Chatterjee AK, Duttagupta SP, Mukherji S. Strain specificity in antimicrobial activity of silver and copper nanoparticles. *Acta Biomater*. 2008;4(3):707–716. doi:10.1016/j.actbio.2007.11.006
23. Kar S, Bagchi B, Kundu B, et al. Synthesis and characterization of Cu/Ag nanoparticle loaded mullite nanocomposite system: a potential candidate for antimicrobial and therapeutic applications. *Biochim Biophys Acta*. 2014;1840(11):3264–3276. doi:10.1016/j.bbagen.2014.05.012
24. Cabiscol E, Tamarit J, Ros J. Oxidative stress in bacteria and protein damage by reactive oxygen species. *Int Microbiol*. 2000;3(1):3–8.
25. Yang Y, Zhang C, Hu Z. Impact of metallic and metal oxide nanoparticles on wastewater treatment and anaerobic digestion. *Environ Sci Process Impacts*. 2013;15(1):39–48.
26. Dodd NJ, Jha AN. Photoexcitation of aqueous suspensions of titanium dioxide nanoparticles: an electron spin resonance spin trapping study of potentially oxidative reactions. *Photochem Photobiol*. 2011;87(3):632–640. doi:10.1111/j.1751-1097.2011.00897.x
27. Zhang L, Zhang Z, He X, Zheng L, Cheng S, Li Z. Diminished inhibitory impact of ZnO nanoparticles on anaerobic fermentation by the presence of TiO2 nanoparticles: phenomenon and mechanism. *Sci Total Environ*. 2019;647:313–322. doi:10.1016/j.scitotenv.2018.07.468
28. Dutta RK, Nenavathu BP, Gangishetty MK, Reddy AV. Studies on antibacterial activity of ZnO nanoparticles by ROS induced lipid peroxidation. *Colloids Surf B Biointerfaces*. 2012;94:143–150. doi:10.1016/j.colsurfb.2012.01.046
29. Piao MJ, Kang KA, Lee IK, et al. Silver nanoparticles induce oxidative cell damage in human liver cells through inhibition of reduced glutathione and induction of mitochondria-involved apoptosis. *Toxicol Lett*. 2011;201(1):92–100. doi:10.1016/j.toxlet.2010.12.010
30. Saddick S, Afifi M, Abu Zinada OA. Effect of Zinc nanoparticles on oxidative stress-related genes and antioxidant enzymes activity in the brain of Oreochromis niloticus and Tilapia zillii. *Saudi J Biol Sci*. 2017;24(7):1672–1678. doi:10.1016/j.sjbs.2015.10.021
31. O'Brien-Simpson NM, Veith PD, Dashper SG, Reynolds EC. Antigens of bacteria associated with periodontitis. *Periodontol 2000*. 2004;35:101–134. doi:10.1111/j.0906-6713.2004.003559.x
32. Imamura T. The role of gingipains in the pathogenesis of periodontal disease. *J Periodontol*. 2003;74(1):111–118. doi:10.1902/jop.2003.74.1.111
33. Han YW, Ikegami A, Rajanna C, et al. Identification and characterization of a novel adhesin unique to oral fusobacteria. *J Bacteriol*. 2005;187(15):5330–5340. doi:10.1128/JB.187.15.5330-5340.2005
34. Abdullah Al M, Sugimoto S, Higashi C, Matsumoto S, Sonomoto K. Improvement of multiple-stress tolerance and lactic acid production in *Lactococcus lactis* NZ9000 under conditions of thermal stress by heterologous expression of *Escherichia coli* DnaK. *Appl Environ Microbiol*. 2010;76(13):4277–4285. doi:10.1128/AEM.02878-09
35. Sasaki-Imamura T, Yano A, Yoshida Y. Production of indole from L-tryptophan and effects of these compounds on biofilm formation by *Fusobacterium nucleatum* ATCC 25586. *Appl Environ Microbiol*. 2010;76(13):4260–4268. doi:10.1128/AEM.00166-10
36. Cui X, Huang C, Zhang M, et al. Enhanced osteointegration of poly (methylmethacrylate) bone cements by incorporating strontium-containing borate bioactive glass. *J R Soc Interface*. 2017;14:131. doi:10.1098/rsif.2016.1057
37. Qiao S, Cao H, Zhao X, et al. Ag-plasma modification enhances bone apposition around titanium dental implants: an animal study in Labrador dogs. *Int J Nanomedicine*. 2015;10:653–664. doi:10.2147/IJN.S73467
38. Zhang W, Wang G, Liu Y, et al. The synergistic effect of hierarchical micro/nano-topography and bioactive ions for enhanced osseointegration. *Biomaterials*. 2013;34(13):3184–3195. doi:10.1016/j.biomaterials.2013.01.008